

Conformations of O_3–F 1:1 Complexes. An Ab Initio Study

Hossein Roohi* **and Batol Mackiabadi**

Department of Chemistry, Faculty of Science, University of Sistan & Balouchestan, P. O. Box 98135-674, Zahedan, Iran

Received January 5, 2007; E-mail: hroohi@hamoon.usb.ac.ir

The conformational geometries of the FO_3 complexes were investigated computationally in the doublet state. Geometry optimization and frequency calculations were performed at the CCSD/aug-cc-pVDZ, CCSD/6-311+G(d) and QCISD/aug-cc-pVDZ levels of theory. To improve the energies, single point calculations were carried out based on the CCSD/aug-cc-pVDZ, QCISD/aug-cc-pVDZ, and CCSD/6-311+G(d) geometries using the CCSD(T), QCISD(T), and CASSCF methods. One non-planar and two planar conformational geometries of the FO_3 complex were found in the doublet state. From energy analysis, the planar geometry with a dihedral angle ($\phi_{O1O2O3F}$) of 0.0° was the most stable one. In addition, vibrational frequencies obtained by CCSD and QCISD methods confirm that the planar geometry of the complex is similar to that reported under the experimental conditions. Quantum theory of Atom In Molecule (QTAIM) was also employed to characterize the electronic properties of the conformational geometries of FO_3 complex.

Halogenated source gases containing X atoms, such as chlorofluorocarbons (CFCs), release X atoms in the atmosphere. Following the release of X atoms, XO radicals form from a fast reaction with ozone: $X + O_3 \rightarrow XO + O_2$ (X = F, Cl, Br, and I). XO radicals may then be involved in a number of multi-step cycles that lead to ozone depletion.[1,2] A rate constant k of $2.2 \times 10^{-11} \exp(-230 \pm 200/T)\,cm^3\,mol^{-1}\,s^{-1}$ for the reaction $F + O_3 \rightarrow FO + O_2$ over the temperature range 200–300 K has been determined by varying of the electronic energies during the approach of the reactants.[1]

The ozone reactions have been the subject of numerous investigations.[1–17] Zhang et al.[13,14] have reported a crossed molecular beam study of the X (Cl, Br) + O_3 reactions. They have concluded that the X (Cl, Br) + O_3 reactions have a direct reaction mechanism and the X atom most likely abstracts a terminal O atom of ozone molecule. Although a great deal of research has been performed in the area of reaction kinetics, the role of intermediates, such as asymmetrical XO–O_2 association complexes, in the atmospheric cycle remains poorly understood. Only the stabilized complex FO_3 in dilute mixtures of F_2 and O_3 in solid argon, for the first time, has been detected by FT-IR spectroscopy.[18] The observed complex is characterized by two intense absorption bands at 1522 and 968 cm^{-1}. The quantum chemical study of the reaction mechanism of ozone and fluorine at the MP2/6-31G(d) level performed by Li et al.[19] show that conformers of FO_3 complex with $\phi_{OOOF} = 0.0$, 85.2, and 81.0° are transition states and an intermediate, respectively. Recently, Nebot-Gil and Peiro-Garcia[20] have theoretically studied the mechanism of the F + O_3 reaction. They have located the same minimum energy structure reported by Li et al. on the potential energy surface at QCISD/6-311+G(d,p) level of theory. From comparison of vibrational frequencies obtained by QCISD/6-311+G(d,p) level and corresponding experimental values in argon matrix, they have concluded that FO_3 QCISD structure (and the MP2 one[19]) can not be the complex reported in argon matrix.[18] To our knowledge, no theoretical works have predicted the structure of most stable conformer of FO_3 complex formed in experimental conditions.

In this study, we computationally investigated the structural, electronic, and infrared spectroscopic properties of the conformations of FO_3 complexes at the CCSD/aug-cc-pVDZ, CCSD/6-311+G(d), and QCISD/aug-cc-pVDZ levels of theory. To improve the energies, single point calculations were carried out based on the CCSD/aug-cc-pVDZ, CCSD/6-311+G(d), and QCISD/aug-cc-pVDZ geometries using the CCSD(T), QCISD(T), and CASSCF methods.

Computational Methods

All of the structures studied in this work were optimized at CCSD/6-311+G(d), CCSD/aug-cc-pVDZ, and QCISD/aug-cc-pVDZ levels of theory. The frequency calculations were performed to characterize stationary points and to calculate the zero-point and thermal energies. To improve the energies, single point calculations were carried out using the CCSD(T) and QCISD(T) methods and aug-cc-pVDZ aug-cc-pVTZ basis sets. All computations were performed using the Gaussian-98 program package[21] on a Pentium 4 computer. Due to the insufficient memory in the computer, geometry optimization at QCISD/aug-cc-pVTZ and CCSD/aug-cc-pVTZ levels of theory could not be performed. In addition, topological properties were calculated using the AIM method on the wavefunctions obtained at CCSD/aug-cc-pVDZ level by AIM2000 program package.[22]

Results and Discussion

Energetics and Geometries. Similar to the X (Cl, Br) reactions,[13,14] it seems that the reaction of F atom with O_3 molecule is a direct reaction and the F atom most likely attacks the terminal oxygen atom. When the F atom attacks the O_3 molecule, three pathways are possible to abstract an oxygen atom: two in-plane approaches, which lead to formation of structures **1b** and **1c**, and an out-of-plane approach, which leads to formation of structure **1a** (Scheme 1).

Published on the web October 12, 2007; doi:10.1246/bcsj.80.1914

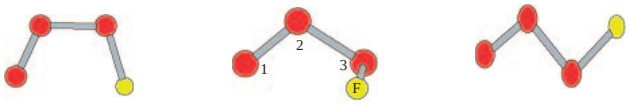

1c(C_s) **1a(C_1)** **1b(C_s)**

Scheme 1.

Table 1. Computed Complexation Energies (kJ mol^{-1}) of Structures **1a**–**1c**

	ΔE_e[a)]	ΔE[b)]	ΔH[b)]	ΔE_e[a)]	ΔE[d)]	ΔH[d)]
	CCSD/aug-cc-pVDZ			CCSD(T)/aug-cc-pVDZ//A[c)]		
1a	−79.7	−71.0	−73.5	−63.5	−54.8	−57.3
1b	−82.5	−74.6	−77.0	−65.6	−57.7	−60.2
1c	−89.7	−77.6	−82.5	−80.2	−68.1	−73.0
	QCISD/aug-cc-pVDZ			QCISD(T)aug-cc-pVDZ//B[c)]		
1a	−81.5	−76.1	−78.5	−73.7	−68.3	−70.8
1b	−85.3	−74.8	−77.2	−81.9	−71.3	−73.8
1c	−94.7	−81.9	−84.4	−100.8	−88.0	−90.5
	CCSD/6-311+G(d)			CCSD(T)/6-311+G(d)//C[c)]		
1a	−67.2	−62.9	−65.4	−47.7	−43.4	−45.9
1b	−67.0	−61.2	−63.7	−47.5	−41.8	−44.2
1c	−71.4	−64.2	−66.7	−61.5	−54.3	−56.8
	QCISD(T)/aug-cc-pVTZ//B[c)]					
1a	−84.7	−79.2	−81.7			
1b	−76.2	−65.7	−68.1			
1c	−107.2	−94.4	−96.9			

a) Electronic complexation energy. b) Relative energy and enthalpy values include ZPE and thermal corrections at 298.15 K. c) A, B, and C are CCSD/aug-cc-pVDZ, QCISD/aug-cc-pVDZ, and CCSD/6-311+G(d) levels of theory, respectively. d) Single point energies have been corrected with zero-point and thermal energies.

The calculated interaction energies, including ZPE and thermal corrections of the conformational geometries of FO_3 complex, are listed in Table 1. The CCSD and QCISD methods predicted that the structures corresponded to a minimum with the exception of QCISD method for **1a**, which confirms that this structure is a transition state with an imaginary frequency of 340.4i cm^{-1}. As can be seen from Table 1, at all levels of theory, structure **1c** was more stable than **1a** and **1b**, and all of the structures were more stable than the separated reactants F and O_3.

Spin contamination problems are inherent to the UHF formalism; whereas the UHF wavefunction is an eigenfunction of $\hat{S}_Z$, it is not an eigenfunction of $\hat{S}^2$. There are a number of higher order spin states (quartets, sextets, etc.) which contaminate $\langle\hat{S}^2\rangle$. The amount of spin contamination for UHF or a correlation corrected ab initio method based on UHF wavefunction is given by the expectation value of the $\hat{S}^2$ operator, $\langle\hat{S}^2\rangle$. The theoretical value for a pure doublet spin state was 0.75. Although, $\langle\hat{S}^2\rangle$ expectation value calculated at the UCCSD/aug-cc-pVDZ and UQCISD/aug-cc-pVDZ levels of theory for structures **1b** and **1c** was 0.7502, its value for **1a** was 0.796 and 0.866, respectively. Thus, the energies and geometries calculated by using the UCCSD and UQCISD methods for structures **1b** and **1c** are reliable.

Table 2. Calculated Reaction Enthalpy and Gibbs Free Energies (kJ mol^{-1}) for $F + O_3 \rightarrow OF\ (^2\Pi) + O_2\ (^3\Sigma_g^-)$

Method	ΔH[a)]	ΔG[a)]
CCSD/aug-cc-pVDZ	−161.8	−169.7
CCSD(T)/aug-cc-pVDZ	−122.9	−131.3
CCSD/6-311+G(d)	−161.8	−169.7
CCSD(T)/6-311+G(d)	−120.8	−129.2
QCISD)/aug-cc-pVDZ	−160.5	−166.8
QCISD(T)/aug-cc-pVDZ	−119.5	−125.8

a) All energy values include zero-point and thermal energies at 298.15 K.

Because of highly multi-configurational nature of ozone, use of MCSCF methods, such as CASSCF, and multi-reference methods, such as CASPT2, to predict the stability of conformers may be essential. Geometry optimization by using Gaussian package at CASSCF and CASPT2 levels on a computer Pentium 4 with CPU 3.2 GHz and RAM 2.0 GB is impossible. Thus, a single point calculation was performed at CASSCF/aug-cc-pVDZ and CASSCF/aug-cc-pVTZ levels of theory on the geometries obtained at level of CISD/aug-cc-pVDZ. The calculated energies for conformers **1a**–**1c** at CASSCF(17,12)/aug-cc-pVDZ level are −323.898093, −323.896979, and −323.903777 a.u., respectively, and at CASSCF(17,12)/aug-cc-pVTZ level are −323.979602, −323.978162, and −323.984009 a.u., respectively. It is evident that conformer **1c** at both levels is more stable than the other two conformers.

The calculated reaction energies by CCSD and CCSD(T) methods for reaction $F + O_3 \rightarrow OF\ (^2\Pi) + O_2\ (^3\Sigma_g^-)$ are given in Table 2. The CCSD(T)/aug-cc-pVDZ and QCISD(T)/aug-cc-pVDZ calculated enthalpies for this reaction (−122.9 and −119.5 kJ mol^{-1}, respectively) are in good agreements with experimental enthalpy[1] (−112.9 kJ mol^{-1}) and the corresponding values of G3 (−111.3 kJ mol^{-1}), G3MP2 (−112.8 kJ mol^{-1})[19] and QCISD(T)/6-311+G(d,p) (−119.5 kJ mol^{-1})[20] levels of theory.

The oxygen atom involved in a possible interaction is referred to here as O3. As can be seen from Table 3, **1a** in the doublet state has a non-planar structure (C_1), whereas **1b** and **1c** have planar structures (C_s) with dihedral angles of 81.7, 180.0, and 0.0°, respectively, at CCSD/aug-cc-pVDZ level. The O3–F and O2–O3 bond lengths in **1c** were, respectively, shorter and longer than corresponding bonds of **1a** and **1b**. In all conformers, the O2–O3 distance was consistently longer than the O1–O2 one. When the O–O distances in the conformers of FO_3 complex and isolated ozone compound (1.259 Å) are compared, complexation causes a lengthening of both the O2–O3 and O1–O2 bonds in the **1a**–**1c**. The amount of the bond length elongation of O2–O3 bond was greater than O1–O2 bond upon complexation. The value of elongation of O2–O3 bond length increased in going from structure **1a** to **1c** by 0.229, 0.369, and 0.471 Å, respectively. In addition, the O1–O2 and O3–F bond lengths changed by +0.048 and +0.049, +0.009 and +0.040, and −0.002 and +0.025 Å, as

Table 3. Optimized Geometrical Parameters of Structures **1a–1c** at (1) CCSD/aug-cc-pVDZ, (2) QCISD/aug-cc-pVDZ, and (3) CCSD/6-311+G(d) Levels[a)]

	1a (C_1)			**1b** (C_s)			**1c** (C_s)		
Parameter	**1**	**2**	**3**	**1**	**2**	**3**	**1**	**2**	**3**
O1–O2	1.266(1.259)[d)] (1.211)[b)]	1.255	1.238	1.227	1.232	1.218	1.209	1.216	1.200
O2–O3	1.488(1.259)[d)]	1.556	1.548	1.628	1.631	1.622	1.730	1.717	1.745
O3–F	1.413 (1.367)[c)]	1.408	1.403	1.407	1.411	1.39	1.392	1.398	1.378
O1–O2–O3	109.7(117.3)[d)]	110.0	111.1	107.8	108.0	108.5	110.5	110.4	111.5
O2–O3–F	102.6	102.1	103.1	100.6	100.6	101.4	99.4	99.3	100.5
O1–O2–O3–F	81.7	70.5	73.2	180.0	180.0	180.0	0.0	0.0	0.0

a) Geometrical parameters of the monomers are given in parentheses. Bond lengths are given in angstroms and angles in degrees. b) For O_2 molecule. c) For OF molecule. d) For O_3 molecule.

Table 4. Calculated Harmonic Vibrational Wavenumbers (Not Scaled)

	Wavenumber/cm^{-1}		
	CCSD/aug-cc-pVDZ	CCSD/6-311+G(d)	QCISD/aug-cc-pVDZ
1a	96.7, 360.0, 510.5, 665.0, 1046.0, 1191.1	48.6, 264.9, 447.1, 637.5, 916.0, 1274.8	340.4i, 80.65, 381.2, 610.0, 1082.2, 1206.1
1b	53.4, 253.8, 328.1, 708.1, 1006.1, 1380.8	33.0, 262.9, 294.4, 691.6, 1001.2, 1399.3	55.6, 246.0, 339.4, 713.9, 970.3, 1345.6
1c	142.3, 278.1, 411.2, 617.1, 996.4, 1489.2	112.3, 257.8, 337.4, 610.4, 1005.4, 1514.1	159.1, 280.6, 450.1, 620.0, 978.3, 1431.2
O_2	1641.5	1667.2	1552.5
OF	1022.6	1048.7	991.6

compared with those of O_2 and OF monomers, for structures **1a–1c**, respectively. From comparison of the O1–O2–O3 bond angle in the isolated ozone (117.3°) and conformers **1a–1c**, it can be seen that the value of this angle decreased upon complexation. The value of the bond angle reduction in **1c** was greater than the **1a** and **1b**.

The calculated vibrational frequencies are given in Table 4. For most stable structure **1c**, the O–O and O–F stretching vibrational frequencies at CCSD/aug-cc-pVDZ level were 1489.2 and 996.4 cm^{-1}, respectively. These frequencies were red-shifted by 152.3 and 26.3 cm^{-1} from the isolated O_2 (1641.5 cm^{-1}) and OF (1022.71 cm^{-1}) molecules, respectively. The red shift in vibrational frequencies with respect to monomers is in agreement with the bond lengthening of O–O and O–F bonds upon complexation.

The predicted conformational geometries were characterized by two intense infrared bands obtained for OF and O_2 at above-mentioned levels. For comparison of calculated and observed frequencies, the scale factors were determined for stretching vibration of OF and O_2 molecules. The calculated scale factors for OF and O_2 vibrations at CCSD/aug-cc-pVDZ level using the observed values of $\nu_{exp}(OF) = 1033$ and $\nu_{exp}(O_2) = 1556\,cm^{-1}$ in solid argon[18] were 1.010 and 0.948, respectively. Using these scale factors, the corrected O–F and O–O stretching vibrational frequencies at CCSD/aug-cc-pVDZ level were 1056.6 and 1129.2, 1016.3 and 1309.0, and 1006.4 and 1411.7 cm^{-1} for structures **1a–1c**, respectively. As mentioned above, two intense absorption bands at 1522 and 968 cm^{-1} (O–O and O–F stretching wavenumbers, respectively) have been detected by FT-IR spectroscopy for reaction between F atom and O_3 molecule in a solid argon matrix.[18] From a comparison of the observed and the calculated stretching vibrational frequencies at CCSD/aug-cc-pVDZ level, it seems that structure **1c** is the complex reported under the experimental conditions.[18] The QCISD/aug-cc-pVDZ level of theory predicted the same results as that found at CCSD/aug-cc-pVDZ level.

Atoms In Molecules Analysis (AIM). The AIM theory is a powerful tool not only to characterize the electronic properties of the species but also to have a better understanding of the nature of the intermolecular interactions.[23–25]

To gain insight into the nature of complexation, analysis of electron density topology in structures **1a–1c** was performed at CCSD/aug-cc-pVDZ level. The values of charge density (ρ), its Laplacian ($\nabla^2\rho$), local energy density (H_{BCP}), local one electron kinetic energy density (G_{BCP}), the ellipticity (ε) at the bond critical points and distances between bond critical points and attractors are given in Table 5. Figures 1a–1c respectively present the molecular graphs, contour maps of charge density ρ and Laplacian of charge density $\nabla^2\rho$ for structures **1a–1c**. From Table 5, the charge density at O1–O2 BCP for all structures was large and its Laplacian was negative, indicating that the charge density is concentrated in the internuclear region. In other word, the electronic charge density is shared between O1 and O2 nuclei. On the other hand, there was a small charge density at O2–O3 bond critical point

Table 5. Bond Critical Point Data (a.u.) and Distances (a.u.) from BCP to the Nuclei (A and B) Calculated at CCSD/aug-cc-pVDZ Level

A–B	ρ	$\nabla^2\rho$	ε	H	G	C_P–A	C_P–B
1a							
O2–O3	0.2587	0.0622	0.0357	−0.19221	0.20775	1.415	1.397
O1–O2	0.4694	−0.8903	0.0036	−0.59006	0.36749	1.231	1.161
O3–F	0.2928	0.1073	0.1201	−0.21998	0.24679	1.270	1.401
1b							
O2–O3	0.1881	0.1553	0.2124	−0.08231	0.12113	1.561	1.515
O1–O2	0.5190	−1.0592	0.0062	−0.69258	0.42779	1.196	1.122
O3–F	0.2994	0.0361	0.1167	−0.23004	0.23906	1.253	1.406
1c							
O2–O3	0.1167	0.5636	0.2465	−0.01352	0.15443	1.618	1.650
O1–O2	0.5418	−1.1008	0.0130	−0.73846	0.46327	1.159	1.125
O3–F	0.3085	0.0621	0.1074	−0.24745	0.26297	1.235	1.395

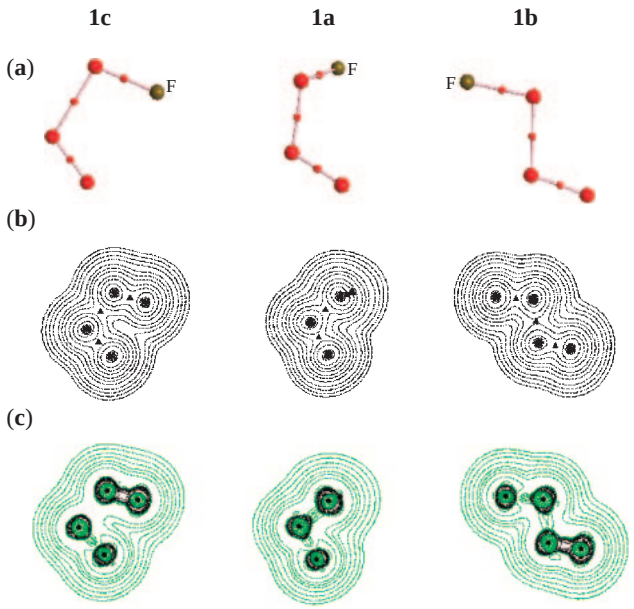

Fig. 1. (a) The molecular graphs of **1a**, **1b**, and **1c**. Nuclei and bond critical points are represented by big and small circles, respectively. (b) Display of the contour maps of charge density in O2–O3–F plane. BCPs are given as triangles. (c) The contour plots of the Laplacian of the charge density in O2–O3–F plane.

and a positive value for its Laplacian, indicating that the electronic charge density is depleted between O2 and O3 nuclei, as expected from complexation between F atom and O_3 molecule. In all cases, charge density, its Laplacian and H_{BCP} at O3–F bond critical points were relatively large and out of the range of values for weak interactions.

It can be seen from Table 5 that, whereas the charge density of O2–O3 bond critical point decreased from **1a** to **1c**, the charge densities of O1–O2 and O3–F bond critical points increased. Thus, the value of charge density at O3–F bond critical point of most stable structure **1c** (0.3085 a.u.) was greater than **1a** (02928 a.u.) and **1b** (0.2994 a.u.) structures. The increase in the charge density at O3–F bond critical point in going from **1a** to **1c** was accompanied by a decrease in the charge density at O2–O3 bond critical point. On the other hand, the $\nabla^2\rho$ value at the O2–O3 bond critical point was found to be positive, indicating that the electronic charge is depleted in the internuclear region. Since the positive value of Laplacian of charge density at O2–O3 bond critical point increased, depletion of charge density in the internuclear region also increased from **1a** to **1c**. Besides, the positive value of $\nabla^2\rho$ at O3–F bond critical point in **1a** (C_1 structure) was greater than that of structure **1c** (C_s structure). As a result, interaction between F atom and O_3 molecule in **1c** is stronger than for **1a**, which is agreement with results obtained from energy analysis. As expected, the shortening of the O3–F bond on going from **1a** to **1c** was accompanied by an increase in ρ and a decrease in positive value of $\nabla^2\rho$ at the associated BCP.

Another quantity used to determine the nature of the interaction is the energy density, H_{BCP}. Unlike the Laplacian, of which the sign is determined by the local virial expression,[25] the sign of H_{BCP} is determined by the energy density itself and is found to be negative for all interactions that result from the accumulation of electron density at the BCP. As can be seen from Table 5, the negative value of H_{BCP} at the O3–F bond critical point of **1c** was bigger than that of **1a**, indicating the greater accumulation of electron density at the associated BCP of **1c** with respect to the **1a**.

In all complexes, the position of critical point at O3–F bond was closer to the atom O3 with a smaller atomic size (see Table 6). In structure **1c**, the distances between bond critical point and nuclei at O3–F bond were smaller than associated distances in **1a** and **1b** structures. In contrast with **1c**, position of the O2–O3 BCP in **1a** moved away from O2 toward O3 atom.

In addition to the local topological properties at the bond critical points, a set of atomic integrated properties, such as atomic electronic population N(Ω), total energy E(Ω) for each atom in a molecule, and atomic volume V(Ω), can be calculated by using topological analysis. The values of integrated atomic properties are reported in Table 6. The electronic population of all O atoms decreased on complexation. The electronic (N) population of O3 and F atoms decreased and increased, respectively, upon complexation, which is an indi-

Table 6. Integrated Atomic Properties (a.u.) Calculated at CCSD/aug-cc-pVDZ Level

A–B	v[a)](A)	v[a)](B)	N(A)	N(B)	E(A)	E(B)
1a						
O2–O3	86.9292	83.9439	7.8444	7.9387	−74.65952	−74.76313
O1–O2	83.9439	107.2638	7.9387	7.9349	−74.76313	−74.79866
O3–F	86.9292	98.1124	7.8444	9.1548	−74.57598	−99.45232
1b						
O2–O3	91.9477	84.6924	7.8906	7.8933	−74.57598	−74.70055
O1–O2	84.6924	107.0509	7.8933	7.9180	−74.70055	−74.86357
O3–F	91.9477	99.2704	7.8906	9.1679	−74.57598	−99.50985
1c						
O2–O3	92.4322	89.1305	7.8139	7.9445	−74.70091	−74.83421
O1–O2	89.1305	102.6096	7.9445	7.9364	−74.83421	−74.74610
O3–F	92.4322	95.0120	7.8139	9.1735	−74.70091	−99.40873

a) For the 0.01 a.u. contour.

cation of charge transfer from O3 to F. The decrease in electronic population of O3 atom in **1c** on complexation was greater than that in **1a**. Because of this greater decrease in electronic population on atom O3 in **1c** relative to **1a**, its atomic energy (−74.10091 a.u.) was smaller than **1a** (−74.57598 a.u.).

Conclusion

The structural and electronic properties of the O_3–F complex formed by reaction of ground state F ($^2P_{3/2}$) atom with ozone molecule in the doublet state were computationally investigated. Structure **1a** in the doublet state has non-planar structure (C_1), whereas structures **1b** and **1c** were planar (C_s). Both CCSD and QCISD method predicted that the stability of **1c** structure is greater than **1a** and **1b** ones and all structures of FO_3 complex are more stable than corresponding monomers.

The values of O–O and O–F stretching vibrational frequencies was red-shifted from the isolated O_2 and OF molecules. From comparison of observed and calculated stretching vibrational frequencies, it seems that the **1c** structure is the complex reported under the experimental conditions.

Topological analysis of electron density at CCSD/aug-cc-pVDZ level showed that the charge density at O1–O2 BCP for all structures was large and its Laplacian was negative, indicating that the charge density is concentrated in the internuclear region. On the other hand, there was a small charge density at the O2–O3 bond critical point and a positive value for its Laplacian, indicating that the electronic charge density is depleted between O2 and O3 nuclei, as expected from complexation between F atom and O_3 molecule. The negative value of H_{BCP} at O3–F bond critical point of **1c** was bigger than that of **1a**, indicating greater accumulation of the electron density at the associated BCP of **1c** with respect to the **1a**.

In all of the structures, the position of critical point at O3–F BCP was located closer to atom O3, which has smaller atomic size. In contrast with **1c**, the position of the O2–O3 BCP in **1a** moved away from O2 toward O3 atom. The electronic (N) population of O3 and F atoms decreased and increased, respectively, upon complexation, which is an indication of charge transfer from O3 to F.

References

1 Y. Bedjanian, G. Poulet, *Chem. Rev.* **2003**, *103*, 4639.

2 R. P. Wayne, *Chemistry of Atmospheres*, Claredon Press, Oxford, **1991**.

3 M.-T. Leu, W. B. DeMore, *Chem. Phys. Lett.* **1977**, *48*, 317.

4 M. A. A. Clyne, H. W. Cruse, *Trans. Faraday Soc.* **1970**, *66*, 2214.

5 J. V. Michael, W. A. Payne, *Int. J. Chem. Kinet.* **1979**, *11*, 799.

6 D. W. Toohey, W. H. Brune, J. G. Anderson, *Int. J. Chem. Kinet.* **1988**, *20*, 131.

7 J. M. Nicovich, K. D. Kreutter, P. H. Wine, *Int. J. Chem. Kinet.* **1990**, *22*, 399.

8 R. Patrick, D. M. Golden, *J. Phys. Chem.* **1984**, *88*, 491.

9 S. S. Prasad, W. M. Adams, *J. Photochem.* **1980**, *13*, 234.

10 W. M. Adams, *Nature* **1980**, *285*, 152.

11 D. L. Baulch, R. A. Cox, R. F. Hampson, Jr., J. A. Kerr, J. Troe, R. T. Watson, *J. Phys. Chem. Ref. Data* **1980**, *9*, 295.

12 D. L. Baulch, R. A. Cox, P. J. Crutzen, R. F. Hampson, Jr., J. A. Kerr, J. Troe, R. T. Watson, *J. Phys. Chem. Ref. Data* **1982**, *11*, 327.

13 J. Zhang, Y. T. Lee, *J. Phys. Chem. A* **1997**, *101*, 6485.

14 J. Zhang, T.-T. Miau, Y. T. Lee, *J. Phys. Chem. A* **1997**, *101*, 6922.

15 H. Grothe, H. Willner, *Angew. Chem., Int. Ed. Engl.* **1994**, *33*, 1482.

16 A. Rauk, E. Tschuikov-Roux, Y. Chen, M. P. McGrath, L. Radom, *J. Phys. Chem.* **1993**, *97*, 7947.

17 S. C. Farantos, J. N. Murrell, *Int. J. Quantum Chem.* **1978**, *14*, 659.

18 E. Y. Misochko, A. V. Akimove, C. A. Wight, *J. Phys. Chem.* **1999**, *103*, 7972.

19 L.-C. Li, J. Wang, X. Wang, A.-M. Tian, N.-B. Wong, *Int. J. Quantum Chem.* **2002**, *87*, 288.

20 J. Peiró-Garcia, I. Nebot-Gil, *Chem. Phys. Lett.* **2004**, *391*, 195, and references therein.

21 M. J. Frisch, G. W. Trucks, H. B. Schlegel, G. E. Scuseria, M. A. Robb, J. R. Cheeseman, V. G. Zakrzewski, J. A. Montgomery, Jr., R. E. Stratmann, J. C. Burant, S. Dapprich,

J. M. Millam, A. D. Daniels, K. N. Kudin, M. C. Strain, O. Farkas, J. Tomasi, V. Barone, M. Cossi, R. Cammi, B. Mennucci, C. Pomelli, C. Adamo, S. Clifford, J. Ochterski, G. A. Petersson, P. Y. Ayala, Q. Cui, K. Morokuma, D. K. Malick, A. D. Rabuck, K. Raghavachari, J. B. Foresman, J. Cioslowski, J. V. Ortiz, A. G. Baboul, B. B. Stefanov, G. Liu, A. Liashenko, P. Piskorz, I. Komaromi, R. Gomperts, R. L. Martin, D. J. Fox, T. Keith, M. A. Al-Laham, C. Y. Peng, A. Nanayakkara, C. Gonzalez, M. Challacombe, P. M. W. Gill, B. Johnson, W. Chen, M. W. Wong, J. L. Andres, C. Gonzalez, M. Head-Gordon, E. S. Replogle, J. A. Pople, *Gaussian 98, Revision A.7*, Gaussian, Inc., Pittsburgh PA, **1998**.

22 F. Biegler-König, J. Schönbohm, D. Bayles, *J. Comput. Chem.* **2001**, *22*, 545.

23 R. F. W. Bader, *Atoms In Molecules. A Quantum Theory*, Clarendon Press, Oxford, U.K., **1990**.

24 R. F. W. Bader, H. Essen, *J. Chem. Phys.* **1984**, *80*, 1943.

25 R. F. W. Bader, *Can. J. Chem.* **1998**, *76*, 973.